Paper No. 47

DEVELOPMENT OF TECHNIQUES FOR ADVANCED OPTICAL CONTAMINATION MEASUREMENT WITH INTERNAL REFLECTION SPECTROSCOPY

J. D. Hayes, *Physicist, Teledyne-Brown Engineering, Huntsville, Alabama;* R. G. Richmond, *Aerospace Technologist, Research and Development Section, NASA-Johnson Space Center, Houston, Texas;* N. E. Chatterton, *Manager, Research Department, Teledyne-Brown Engineering, Huntsville, Alabama*

ABSTRACT

A program has been undertaken at the National Aeronautics and Space Administration (NASA) - Johnson Space Center (JSC) to develop and evaluate diagnostic instrumentation for the measurement of molecular contamination in space simulation chambers. This paper describes a technique of monitoring volatile contaminants in a large space simulation chamber using internal reflectance spectroscopy. The analytical phase included: (1) parameter effects determination (film thickness, sample absorption, refractive index variation, chemical reactions, film homogenity, polarization, etc.), (2) thin film/thick film/bulk sample optimization analysis, (3) optical properties of candidate internal reflectance element (IRE) materials, (4) IRE design considerations, and (5) potential system range and sensitivity. Three IRE's were fabricated. Experimental results of IRE infrared spectra for six potential contaminants are reported.

INTRODUCTION

Increased complexity of space-vehicle designs and experiments have resulted in significantly more stringent cleanliness requirements for space-environment testing and simulation facilities. Although some vehicles and experiments are relatively insensitive to contamination, many spacecraft contain systems and components that are ultrasensitive to contamination (particularly molecular contamination, as from backstreaming of vacuum-pump oils, outgassed paints, and epoxies).

A program has been undertaken at the National Aeronautics and Space Administration (NASA)-Johnson Space Center (JSC) to: (1) define, control, and reduce contamination levels in their space-environment simulation facilities, and (2) minimize these levels within the test-environment requirements. This program logically includes development and evaluation of diagnostic instrumentation. This paper describes the feasibility of monitoring volatile contaminants in a large space simulation chamber using internal reflectance spectroscopy (IRS) techniques.

IRS has been used for several years to identify qualitatively minute quantities of organic compounds. The feasibility of this method for thick film measurements has been widely demonstrated. The feasibility for very thin films, however, has been shown only for a few selected compounds.

This study was directed primarily at determining feasibility of using IRS techniques for identifying, both qualitatively and quantitatively, six specific components known or suspected of contaminating surfaces tested in the space simulation chamber A at the JSC. In performing this study, the method of approach was: (1) to optimize sensitivity and measurement precision, (2) to select internal reflection elements that would not be sensitive to small experimental parameter variations that complicate the analysis, but yet could theoretically detect samples several monolayers thick, and (3) to develop procedures and provide data necessary for correcting the spectra of thick samples with rapidly varying (with wavelength) refractive indices.

The effort was divided into analytical and experimental phases. The analytical phase included: (1) a determination of the effects of several parameters (film thickness, sample absorption, refractive index variation, chemical reactions, film homogeneity, polarization, etc.), (2) an optimization analysis for thin films versus thick films versus bulk samples, (3) determination of optical and physical properties of candidate internal reflectance element (IRE) materials, (4) IRE design considerations, and (5) potential range and sensitivity of an assembled system.

Theoretical Considerations

The optical properties of absorbing media may be described quantitatively by the complex refractive index, $N = n + ik$, where n, the real part of the refractive index, is defined as the ratio of the velocity of light in vacuum, c, to the phase velocity, v,

in the dielectric of a plane electromagnetic wave having constant amplitude along a wave front,

$$n = c/v \ . \tag{1}$$

The imaginary part of the complex refractive index, k, often called the extinction coefficient, describes the damping of the wave as it traverses the absorbing medium, and is defined by the relation

$$E = E_0 \exp\left(-\frac{2\pi k z}{\lambda}\right) \tag{2}$$

where

z - coordinate in the direction of propagation
E_0 - amplitude of the electromagnetic wave at $z = 0$
E - amplitude at z
λ - wavelength of the electromagnetic wave in vacuum.

The theory of reflection and transmission of light by thin films has been discussed in many texts. Expressions for the reflectance, R, at a given wavelength are obtained by the application of boundary conditions to Maxwell's equations for a plane electromagnetic wave incident on the boundary between two media.

When a plane wave falls onto a boundary between two homogeneous media of different optical properties, it is split into two waves, a transmitted wave proceeding into the second medium and a reflected wave propagated back into the first medium. The existence of these two waves can be demonstrated from the boundary conditions, since it is easily seen that these conditions cannot be satisfied without postulating both the transmitted and the reflected wave. The transmitted beam is refracted according to Snell's law:

$$n_1 \sin\theta = n_2 \sin\phi \tag{3}$$

where

n_1 - the refractive index in medium 1
n_2 - the refractive index in medium 2
θ - the angle of incidence in medium 1
ϕ - the angle of refraction in medium 2.

For the reflected beam, the angle of reflection is equal to the angle of incidence. The reflected amplitudes for unit incident amplitudes for light with

the electric field vector perpendicular and parallel to the plane of incidence, respectively, are given by Fresnel's equations,

$$R_{\perp} = \frac{n_1 \cos \Theta - n_2 \cos \phi}{n_1 \cos \theta + n_2 \cos \phi} \tag{4}$$

$$R_{\parallel} = \frac{n_2 \cos \theta - n_1 \cos \phi}{n_2 \cos \theta + n_1 \cos \phi} \tag{5}$$

For internal reflection, i.e., when the light approaches the interface from the denser medium, both $R_{\perp}$ and $R_{\parallel}$ become 100 percent at the critical angle θ_c, given by

$$\theta_c = \sin^{-1}\left(\frac{n_2}{n_1}\right) = \sin^{-1} n_{21} \tag{6}$$

where $n_{21} = n_2/n_1$. (Ref. 1).

It can be shown from Maxwell's equations that standing waves are established normal to a totally reflecting surface because of the superposition of the incoming and reflected waves (ref. 2). For total internal reflection, there is a sinusoidal variation of the electric field amplitude with distance from the surface in the denser medium. By selecting the proper angle of incidence, it is possible to locate the antinode (the electric field maximum) at the surface and thus obtain the most efficient energy transfer across the interface. An evanescent wave exists in the rarer medium whose electric field amplitude decays exponentially with distance from the surface (see fig. 1). Consequently, one can define a depth of penetration, d_p (ref. 2) as the distance required for the electric field, E, to fall to 1/e of its d_p value at the surface, E_o, i.e.,

$$E = E_o \exp(-z/d_p) \tag{7}$$

The depth of penetration is given by

$$d_p = \frac{\lambda}{2\pi} \cdot \left(\sin^2 \Theta - n_{21}^2 \right)^{-\frac{1}{2}} \tag{8}$$

When the actual material thickness, d, is much less than d_p, the effective thickness d_e is given by the thin film formula (ref. 1)

$$d_e = \frac{n_{21} E_o^2 d}{\cos \theta} \quad (9)$$

while for $d \gg d_p$, d_e is given by the bulk material formula

$$d_e = \frac{n_{21} E_o^2 d_p}{2 \cos \theta} \quad (10)$$

When d_e is comparable to d_p, equations 9 and 10 are not valid, one must use:

$$d_e = \left(\frac{n_{21}}{\cos \theta}\right) \cdot \left(\frac{E_o^2 d_p}{2}\right) \cdot \left[1 - \exp(-2d/d_p)\right] \quad (11)$$

When the rarer medium is absorbing, the critical angle is not sharply defined and the reflectivity curves become less steep in this region. The absorption loss is quite large near the critical angle, is greater for parallel polarization than it is for perpendicular polarization, and decreases with increasing angle of incidence.

This behavior is the basis for attenuated total reflectance (ATR) spectroscopy, since the internal reflection, particularly in the vicinity of the critical angle, may be extremely sensitive to changes in the absorption coefficient.

The above equations indicate that four factors influence the strength of coupling of the evanescent wave with the absorbing medium. These four factors are the depth of penetration, d_p, the electric field strength at the interface, E_o, the sampling area and the refractive index matching.

The great advantage of ATR spectroscopy is that because of a reflectance of 1 for nonabsorbing media, many reflections can be utilized without reflection losses. Hence, small absorption losses for weakly absorbing films can be multiplied many times without a simultaneous increase in "noise" due to substrate reflection inefficiencies.

IRE Design Considerations

The design of an IRE for real-time contamination detection and indentification considered several trade-offs, the first of which was between maximum detection sensitivity and contaminant identification. The strongest absorption bands for most materials are

found in the vacuum ultraviolet spectral region between 1200 A and 2200 A. Although the gross identifying features characteristic of certain groups of contaminants may be inferred from the recorded spectra in this region, unique identification of single components is difficult and analysis of multicomponent samples is virtually impossible. In addition, materials which are sufficiently transparent in the vacuum ultraviolet have very low refractive indices, which vary rapidly in this spectral region. For the contaminants considered, the sample refractive index exceeds that of the candidate IRE materials. Although the use of thin-film samples may have circumvented this problem, the rapid variation of both the IRE material and the sample refractive indices with incident wavelength also significantly complicates the analysis of spectra in this region.

In the vacuum ultraviolet region, the peak absorption coefficient is not much different than the peak values in the infrared, however, the ultraviolet spectra are more ambiguous than the infrared spectra. In the infrared spectral region, unique identification of individual components is relatively easy and multicomponent analysis is often not much more difficult.

Three element designs were selected for element fabrication based on the analytical results. These included a 46-reflection KRS-5 element for operation at 30 degrees, a 26-reflection germanium element for operation at 35 degrees, and a 26-reflection germanium element for operation at 40 degrees in conjunction with KRS-5 plates as the third optical medium.

Of the many factors affecting ATR spectra (e.g., sample and IRE refractive index variation, chemical reactions of the IRE with atmospheric constituents or with the sample, degree of film homogeneity, incident light polarization, and the degree of collimation) the greatest factor is film thickness.

It may be shown that for any sample thickness, d, the maximum interaction possible is $E_o^2 d$. However, as the actual thickness of the sample is increased, the total interaction will be increased, but may not reach the maximum possible for that particular thickness. As d becomes greater than $0.1\, d_p$, the interaction becomes dependent on wavelength, since d_p is wavelength-dependent. If an interaction efficiency, IE, is defined by

$$IE = \frac{d_p}{2d} \cdot \left[1 - \exp(-2d/d_p)\right] \qquad (12)$$

the wavelength dependence of the interaction can be calculated and plotted as interaction efficiency versus wavelength for various actual film thicknesses, independent of the various other affecting parameters. Although the effect can be shown as a function of d_p/d, it is more relevant to the purposes of this study to plot IE versus wavelength.

Figures 2, 3, and 4 show the variation of IE with wavelength for film thicknesses of 0.01 micrometer (100 A), 0.1 micrometer (1000 A), and 1 micrometer (10,000 A), for IRE materials with refractive indicies of 4.00 (Ge), 2.37 (KRS-5), and 1.98 (AgCl) respectively. These curves can be used to select a maximum film thickness for a particular IRE material such that the wavelength distortion of the absorption bands will be negligible, or alternatively to correct for such distortion, assuming the film thickness is known.

Table 1 summarizes the pertinent optical physical properties of the materials for the infrared spectral region. For the region 2 to 20 micrometers, the materials with most appeal are cesium bromide (N = 1.65), silver bromide (N = 2.3), and germanium (N = 4.0). Cesium bromide has a high solubility in water (124 g/100 g H_2O) and is quite soft. Silver chloride is extremely soft and must be handled and cleaned carefully to avoid surface finish destruction. Silver bromide has low solubility, but is extremely soft. Potassium bromide transmits to about 18 micrometers, but has high solubility. Potassium fluoride and potassium iodide have extended transmission ranges but also are highly soluble. Practically all of the alkali halides have useful optical properties in the infrared spectral region, but almost all are highly soluble and deteriorate in atmospheres with relative humidity greater than 35 percent (ref. 3).

TABLE I.- OPTICAL AND PHYSICAL PROPERTIES
OF INFRARED IRE MATERIALS

Wavelength (μm)	Refractive index				
	CsBr	Si	Ge	KRS-5 25° C	AgCl 23.9° C
0.5	1.71				2.0965
1.0	1.677			2.4462	2.0224
2.0	1.672	3.4534	4.1066	2.3950	2.0062
3.0	1.669	3.4320	4.0452	2.3857	2.0023
4.0	1.668	3.4253	4.0246	2.3820	1.9998
5.0	1.667	3.4223	4.0152	2.3798	1.9975
6.0	1.666	3.4202	4.0100	2.3780	1.9948
7.0	1.665	3.4189	4.0071	2.3763	1.9919
8.0	1.664	3.4184	4.0048	2.3745	1.9885
9.0	1.663	3.4181	4.0038	2.3727	1.9846
10.0	1.662	3.4179	4.0032	2.3707	1.9803
11.0	1.661	3.4176	4.0028	2.3685	1.9756
12.0	1.659	3.4176	4.0024	2.3662	1.9703
13.0	1.658	3.4176	4.0021	2.3637	1.9644
14.0	1.657	3.4176	4.0015	2.3610	1.9581
15.0	1.655	3.4176	4.0014	2.3581	1.9511
16.0	1.653		4.0012	2.3550	1.9436
17.0	1.651			2.3517	1.9354
18.0	1.648			2.3482	1.9266
19.0	1.646			2.3445	1.9171
20.0	1.644			2.3406	1.9069
21.0	1.641			2.3364	
22.0	1.638			2.3321	
23.0	1.635			2.3275	
24.0	1.632			2.3226	
25.0	1.628			2.3176	
26.0	1.625			2.3123	
27.0	1.621			2.3068	
28.0	1.617			2.3010	
29.0	1.614			2.2950	
30.0	1.609			2.2887	

Experimental Results

The spectral response of each of the individual contaminats (Dow Corning DC705, Sun vis 706, Houghto Saf 1120, 3M "Black Velvet" paint - 2 components) for several contaminant thickness using the different IRE's was measured using the experimental geometry shown in figure 5. Several methods of depositing the contaminants were attempted. The most desirable method was to outgas or heat to volatility the contaminant in a vacuum chamber and then deposit the contaminant on the IRE while monitoring the thickness of the deposit with a quartz crystal microbalance (QCM) located adjacent to the IRE. For this experiment, however, the sticking coefficient of the contaminant/IRE interface was determined to be much greater than that of the contaminant/QCM interface. In addition, the QCM exhibited a self-cleaning process when operated during the deposition. The contaminants were successfully applied directly to the IRE from standard acetone and carbon tetrachloride solutions.

A known quantity of the desired solution was dispersed on each reflecting face of the IRE and the solvent allowed to evaporate before the spectra were recorded. The thickness of the deposited film was calculated from the quantity of solution dispersed and the area of the IRE face, assuming a film of uniform thickness. The mass of contaminant deposited was checked by depositing an equal quantity of contaminant on a QCM crystal and measuring the frequency shift after solvent evaporation.

Figures 6 through 12 show ATR specta of the individual contaminants of interest as measured with a 45-degree KRS-5 IRE, in conjunction with a Beckman filter wheel monochromator and a highly convergent (half-angle approximately 20 degrees) incident radiation beam. The incident radiation was unpolarized. For all the measurements except for the mixtures, the 3M Black Velvet coating components were measured separately and after the carbon pigment had been removed from the component. This was done because the Black Velvet coating is an epoxy coating that would ruin the IRE's if allowed to cure. The spectra in figures 6 through 12 are for films approximately 0.6 microns thick on each face of the IRE.

Typical individual spectra of the contaminants on the 35-degree germanium and on the 30-degree KRS-5 IRE's are shown in figures 13 through 18. These spectra were recorded using a McPherson Model 218 grating monochromator with 2-millimeter entrance and exit slits, and converging incident radiation beam of 5-degree half-angle, with the incident radiation

polarized parallel to the plane of incidence of the internal reflections. The films for these spectra were approximately 0.2 micrometer thick. In general, the spectra taken with the latter IRE's show higher resolution and greater sensitivity than do those taken with the 45-degree KRS-5 IRE in a highly convergent radiation beam.

Spectra of DC-704 and Sun vis 706 were recorded for three different film thicknesses and are shown in figures 19 through 22. The thinnest films shown are approximately 220 A thick while the thickest films are approximately 2 micrometers thick. Spectra were also recorded (fig. 23), for some films approximately 20 A thick, although these spectra are not very clean due to a high level of noise in the detector.

Figure 19 shows spectra of three films of DC-704 on the 30-degree KRS-5. As can be seen, both the 175 A film and the 1750 A film are quite adequate for identification, with little or no spectral distortion. However, the 1.75-micrometer film shows almost total absorption for wavelengths greater than 7 micrometers and thus would not be useful for spectral identification. It should be recalled, however, that the 30-degree KRS-5 IRE was designed for thin films primarily and this effect was anticipated. The 35-degree germanium IRE, on the other hand, was designed for thick films as well as for thin films. Figure 20 shows DC-704 spectra on the 35-degree germanium IRE. Note that the 35-degree germanium IRE is not quite as sensitive as the 30-degree KRS-5 IRE (compare the 240 A curve with the 175 A curve on KRS-5) but that the spectra for the thick film (2.4 micrometers) is still very clean and undistorted for the 35-degree germanium IRE.

The same type behavior is demonstrated for Sun vis 706. Figure 21 shows Sun vis 706 on the 30-degree KRS-5 IRE and figure 22 shows Sun vis 706 on the 35-degree germanium IRE. Again the 30-degree KRS-5 IRE shows distortion for the thickest film while the 35-degree germanium IRE exhibits no spectral distortion.

A mixture of 0.2 percent DC-705, 0.2 percent Sun vis 706, 0.2 percent Houghto Saf 1120, and 0.4 percent 3M Black Velvet was prepared and spectra recorded using the 45-degree KRS-5, and the 30-degree KRS-5 IRE's, as before. These spectra are shown in figures 24, and 25. Film thickness on the 45-degree KRS-5 IRE was approximately 0.4 micrometer, while that for the other spectrum was approximately 0.2 micrometer. The improved detail for the 30-degree KRS-5 over the standard 45-degree KRS-5 IRE is readily apparent. The Houghto Saf 1120 contaminant had so many strong

absorption bands that the spectra was difficult to analyze quantitatively.

Conclusions

The experimental results verified the analytical predictions and demonstrated the feasibility of using ATR techniques to detect and identify their contaminant deposits. This work has shown that it is possible to identify contaminants with deposits as thin as 20 A from infrared ATR spectra obtained with a 30 degree, 46-reflection KRS-5 element using radiation polarized parallel to the plane of incidence. It has also demonstrated that thick film or bulk spectra can be obtained undistorted by using a 35-degree, 26-reflection germanium element.

The quantitative analysis of a complex spectrum of a multicomponent mixture yielded the concentrations of the individual components with an accuracy of ±50 percent for the worst masked bands and ±10 percent for the most easily interpretable bands. This example demonstrates the feasibility of quantitative multicomponent mixture analysis. Had the Houghto-Saf 1120, a material with very strong bands across the entire spectral range, been omitted from the mixture, an overall accuracy of ±10 percent could probably have been obtained.

The proposed 40-degree germanium/KRS-5 combination did not perform as well as anticipated, due primarily to the difficulty of maintaining optical contact between the germanium and the KRS-5 with a contaminant present. Also, the KRS-5 is extremely soft and deforms easily so that maintaining the uniform optical contact necessary is impractical.

The 35-degree, 26-reflection germanium element showed high sensitivity with thin films (although not as high as that of the 30-degree KRS-5) and displayed no special distortion with thick films or bulk spectra. In addition, the germanium is easily cleaned and is very hard, making it ideal for use in all applications except those demanding the highest sensitivity.

522-137 O - 73 - 41

REFERENCES

1. Harrick, N. J., Internal Reflection Spectroscopy, Interscience Publishers, New York, 1967

2. Born, M., and E. Wolf, Principles of Optics, Second Edition, MacMillan, New York, pp. 277-281, 1964

3. Harshaw Optical Crystals, Harshaw Chemical Company, 1967

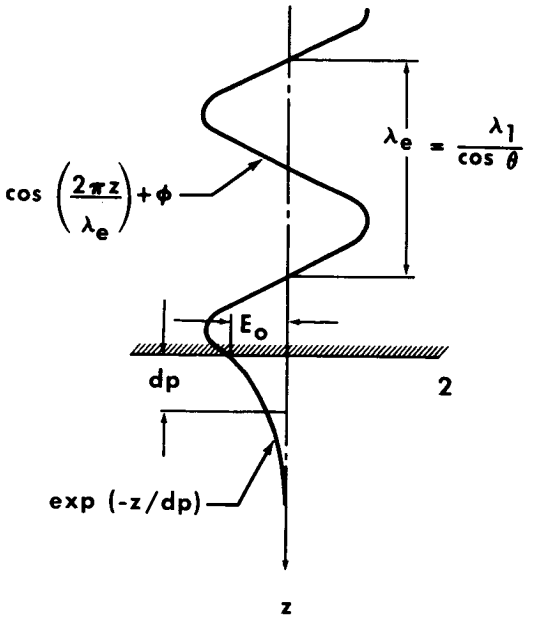

Fig. 1 - Standing wave amplitudes established near a totally reflecting interface (ref. 1)

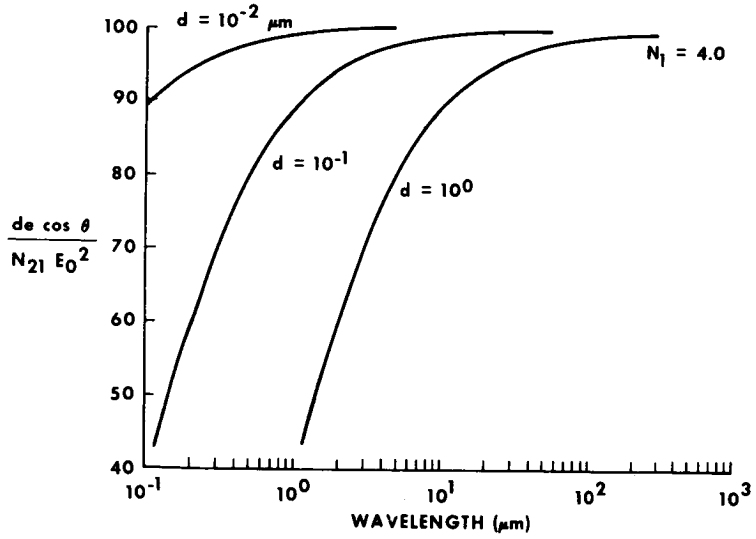

Fig. 2 - Variation of interaction efficiency with wavelength for germanium IRE

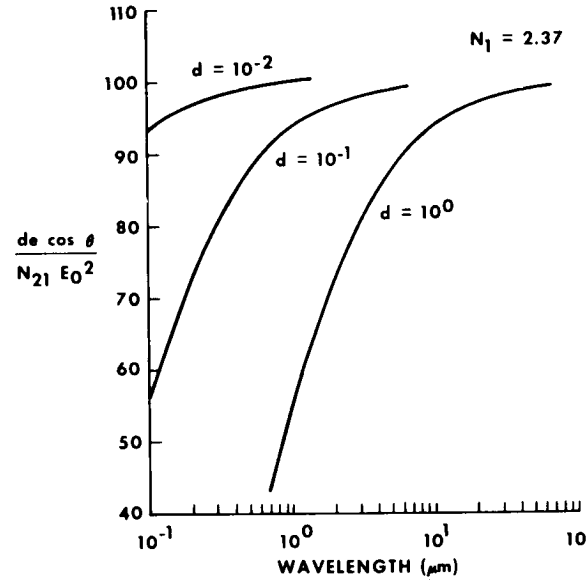

Fig. 3 - Interaction efficiency as a function of wavelength for KRS-5 IRE

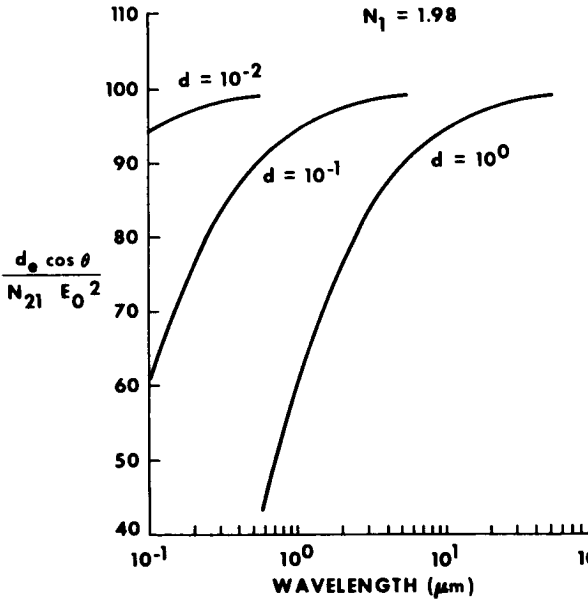

Fig. 4 - Variation of interaction efficiency with wavelength for AgCl IRE

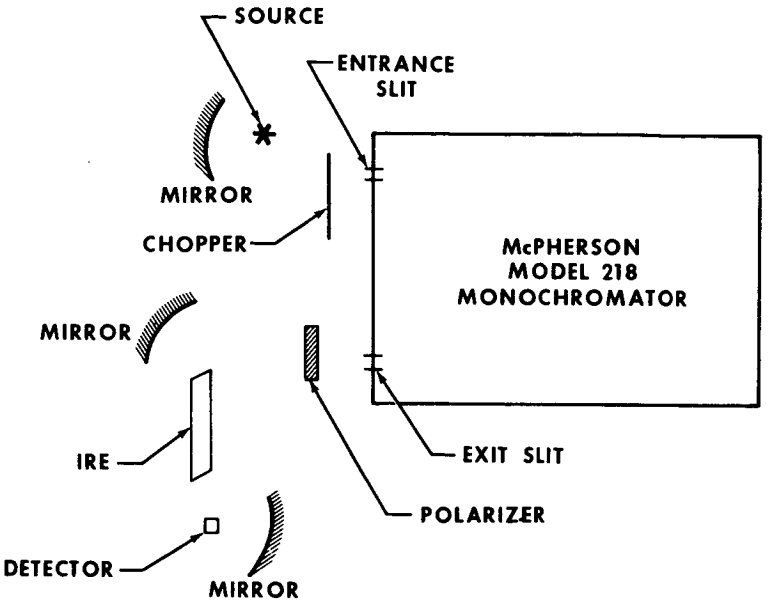

Fig. 5 - Optical schematic of experimental apparatus

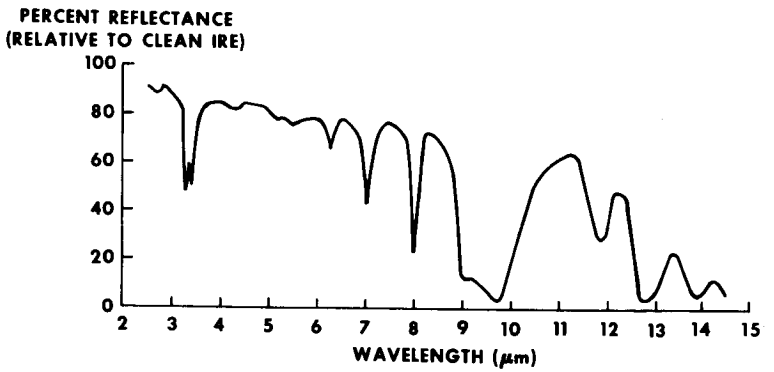

Fig. 6 - DC-704 on 45-degree KRS-5 IRE

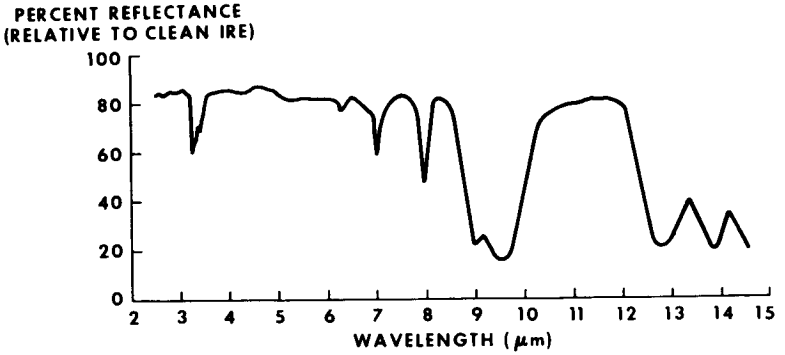

Fig. 7 - DC-705 on 45-degree KRS-5 IRE

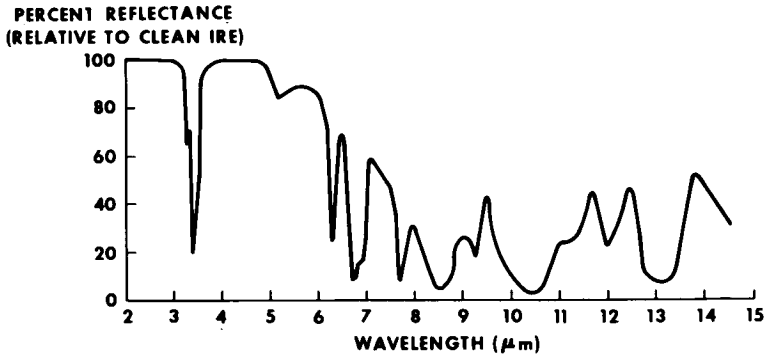

Fig. 8 - Houghto SAF 1120 on 45-degree KRS-5 IRE

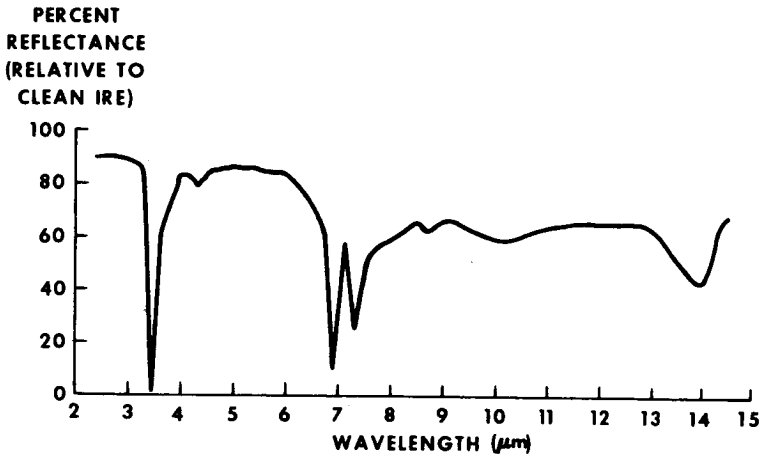

Fig. 9 - Sun vis 706 on 45-degree KRS-5 IRE

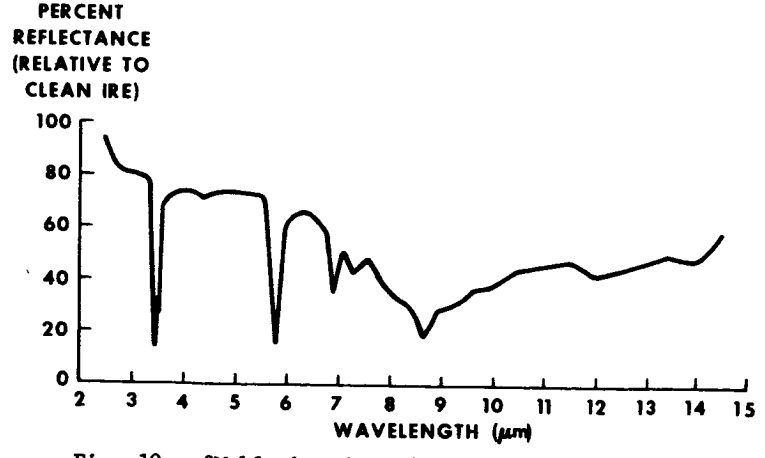

Fig. 10 - 3M black velvet 401-C10 (component I) on 45-degree KRS-5 IRE

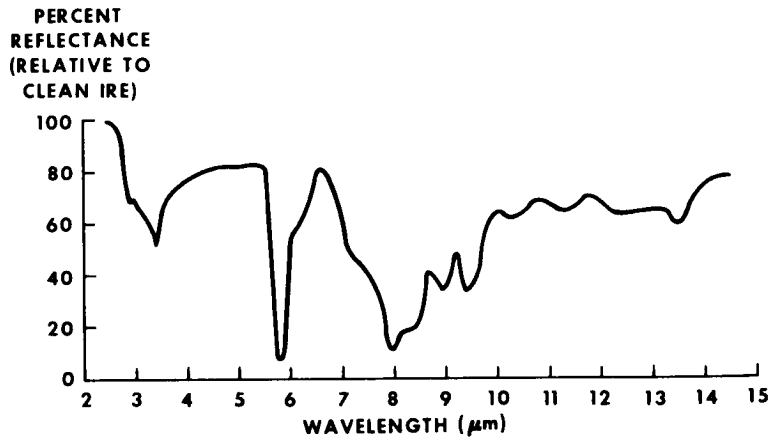

Fig. 11 - 3M black velvet 401 series (component II) on 45-degree KRS-5 IRE

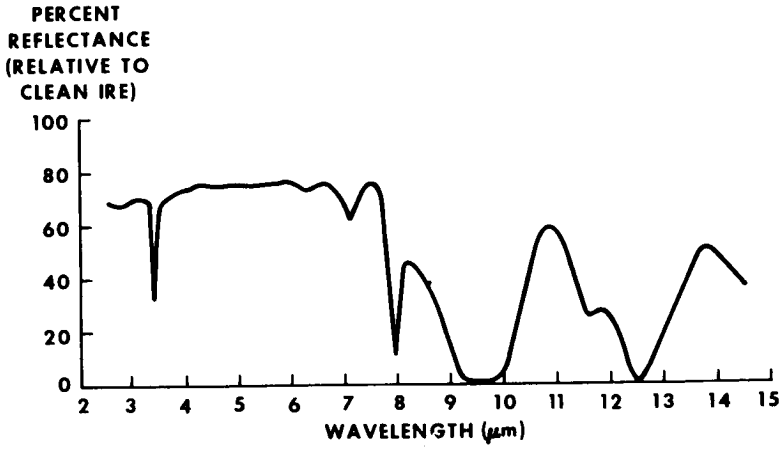

Fig. 12 - DC-11 on 45-degree KRS-5 IRE

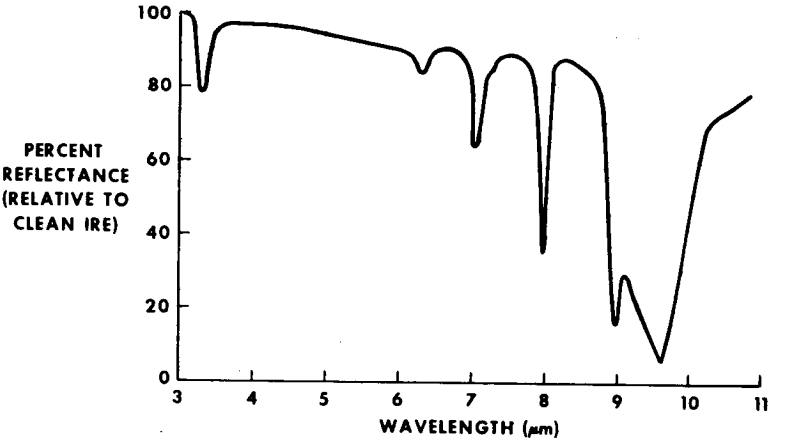

Fig. 13 - DC-704 on 35-degree germanium IRE

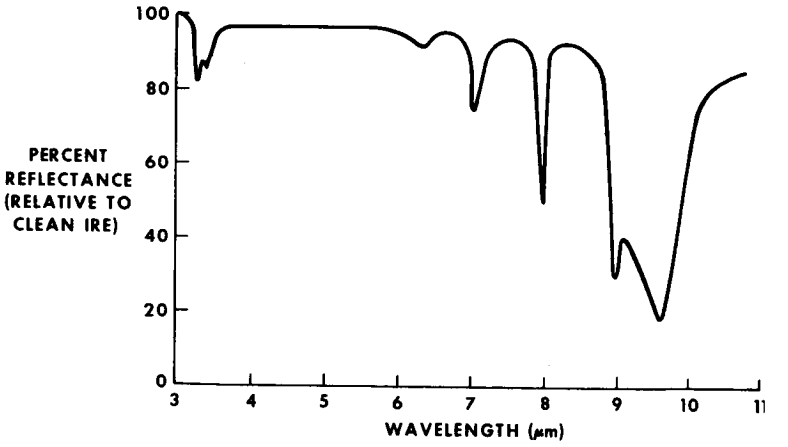

Fig. 14 - DC-705 on 35-degree germanium IRE

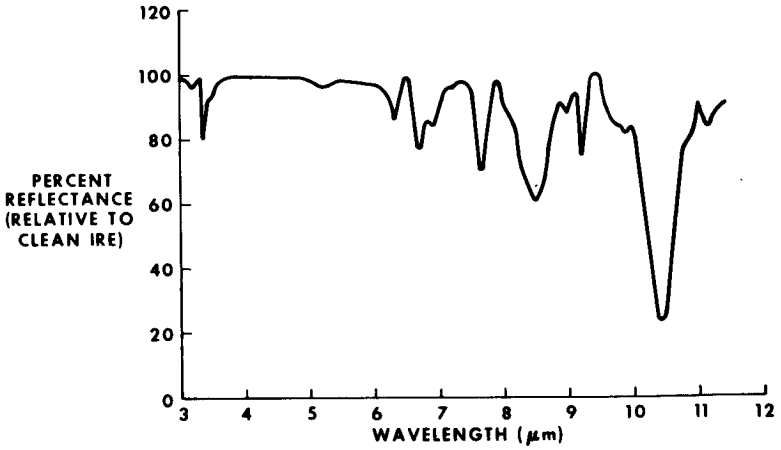

Fig. 15 - Houghto SAF 1120 on 35-degree germanium IRE

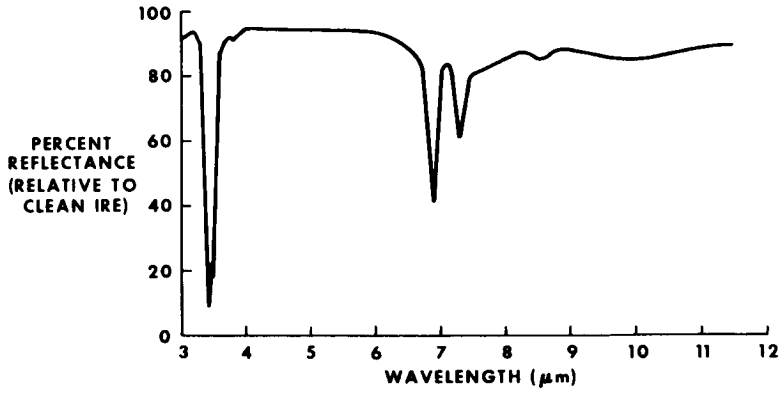

Fig. 16 - Sun vis 706 on 35-degree germanium IRE

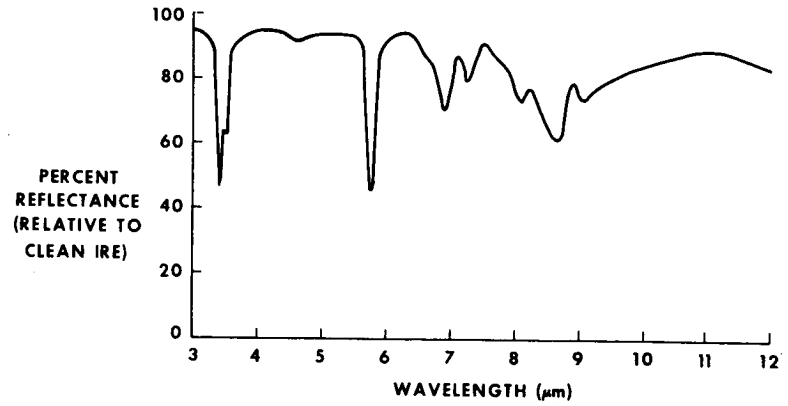

Fig. 17 - 3M black velvet coating 401-C10 (component I) on 35-degree germanium IRE

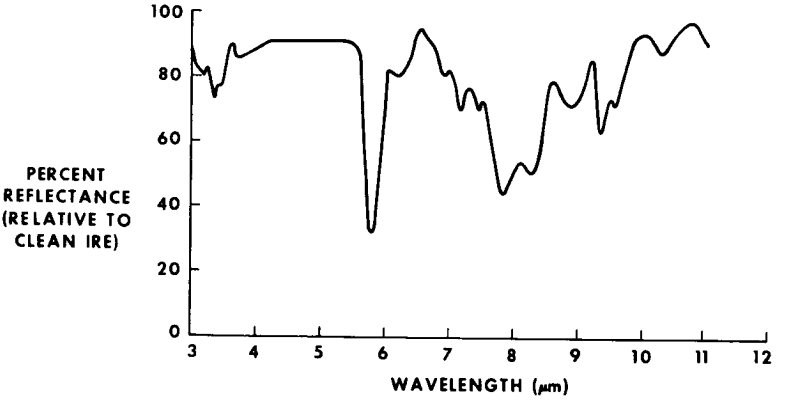

Fig. 18 - 3M black velvet coating 401 series (component II) on 35-degree germanium IRE

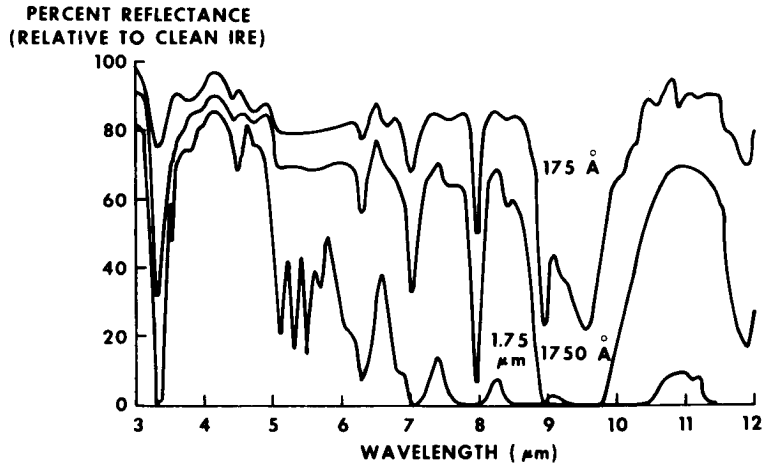

Fig. 19 - Three films of DC-704 on 30-degree KRS-5 IRE

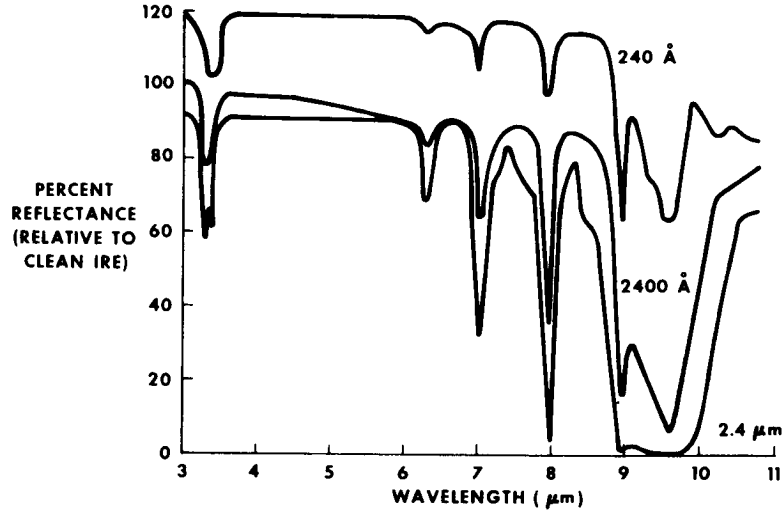

Fig. 20 - Three films of DC-704 on 35-degree germanium IRE

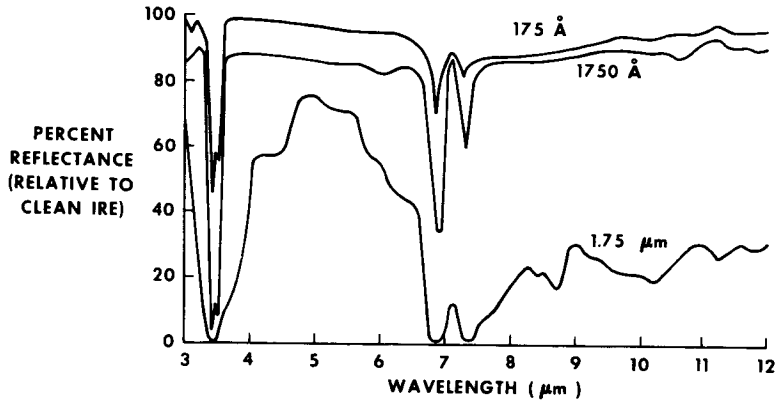

Fig. 21 - Three films of sun vis 706 on 30-degree KRS-5 IRE

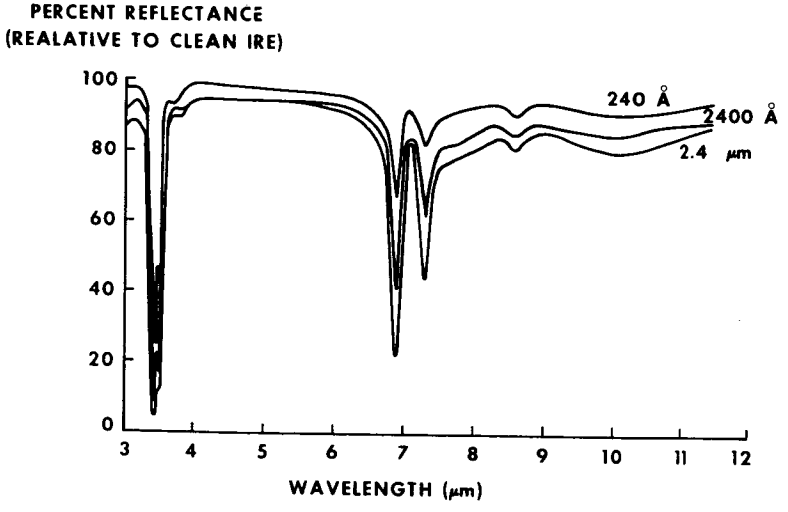

Fig. 22 - Three films of sun vis 706 on 35-degree germanium IRE

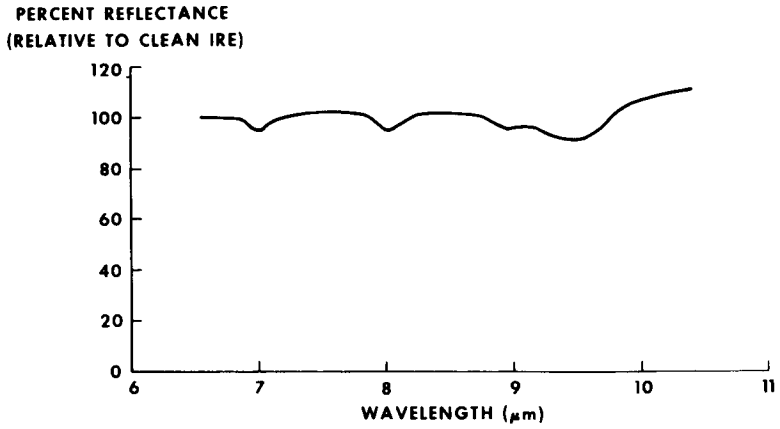

Fig. 23 - 20 A film of DC-705 on 30-degree KRS-5 IRE

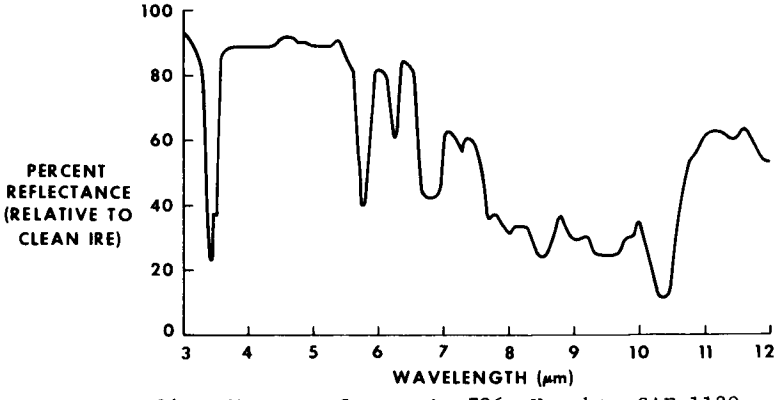

Fig. 24 - Mixture of sun vis 706, Houghto SAF 1120, DC-705, and 3M black velvet on 45-degree KRS-5 IRE

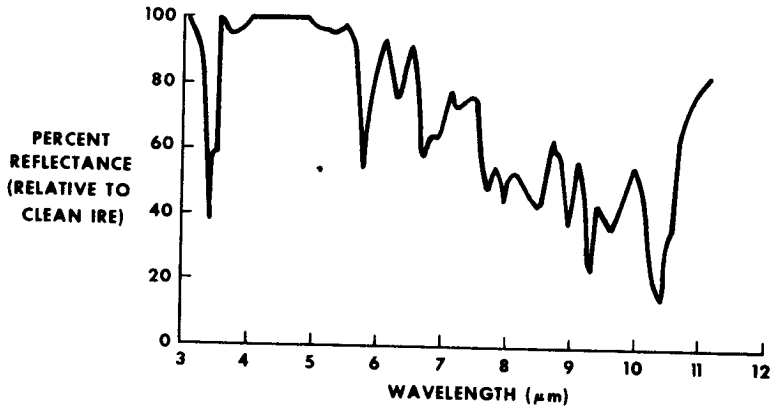

Fig. 25 - Mixture of sun vis 706, Houghto SAF 1120, DC-705, and 3M black velvet on 30-degree KRS-5 IRE